2. Toward a High-Resolution Stable Isotope Stratigraphy of the Last 1.1 m.y.: Site 1144, South China Sea[1]

Christian Bühring,[2] Michael Sarnthein,[2] and
Helmut Erlenkeuser[3]

ABSTRACT

Narrow-spaced oxygen and carbon stable isotope records of the planktonic foraminifer *Globigerinoides ruber* (white) were obtained at Ocean Drilling Program Leg 184 Site 1144 to establish a first record of high-resolution Pleistocene monsoon variability on orbital to centennial timescales in the northern South China Sea. The new records extend from the Holocene back to marine isotope Stage (MIS) 34 (1.1 Ma). Sedimentation rates average 0.56 m/k.y. for the upper Matuyama and Brunhes Chrons and increase to 1.8 m/k.y. over the last 100 k.y. Stable isotope records thus reach an average time resolution of 270–500 yr for the last 375 k.y. and 570 yr further back to 700 ka. On the other hand, major stratigraphic gaps were identified for peak warm Stages 5.5, 7.5 (down to 8.4), 11.3, and 15.5. These gaps probably resulted from short-lasting events of contour current erosion induced by short-term enhanced incursions of Upper Pacific Deep Water near the end of glacial terminations. A further major hiatus extends from MIS 34 to MIS 73(?). The long-term variations in monsoon climate were largely dominated by the 100-k.y. eccentricity cycle. Planktonic $\delta^{13}C$ values culminated near 30, 480, and 1035 ka and reflect an overlying 450-k.y. eccentricity cycle of minimum nutrient concentrations in the surface ocean. Superimposed on the orbital variations, millennial-scale cycles were prominent throughout the last 700 k.y., mainly controlled by short-term changes in monsoon-driven precipitation and freshwater input from

mainland China. During the last 110 k.y. these short-lasting oscillations closely match the record of 1500-yr Dansgaard-Oeschger climate cycles in the Greenland ice core record.

INTRODUCTION

A principal objective for Ocean Drilling Program (ODP) Leg 184 Site 1144 (20.05°N, 117.42°E; water depth = 2037 m) (Fig. F1) was to recover a complete sequence of high-sedimentation-rate hemipelagic sediments from the middle and late Pleistocene to address fundamental questions regarding the paleoenvironment in the South China Sea (SCS) and to reconstruct the history of the East Asian Monsoon on orbital to sub-Milankovitch timescales over the last 1 m.y.

To date, only a few published paleoceanographic records from Southeast Asian marginal seas provide a time resolution sufficient to resolve high-frequency variations in local ocean circulation and paleoclimate. The high accumulation rates at Site 1144 (Fig. F1), retrieved from a thick hemipelagic sediment drift (Sarnthein et al., 1994; Shipboard Scientific Party, 2000) on the northern continental slope of the SCS, offer an unprecedented opportunity to reconstruct Quaternary monsoon variations on millennial to centennial timescales.

Our primary goals are (1) to provide a detailed and reliable high-resolution stable isotope stratigraphy for the northern SCS over the last 1 m.y.; (2) to uncover stratigraphic gaps in centennial to millennial climate oscillations during the Brunhes Chron, with special focus on the last six glacial and interglacial periods; and (3) to compare paleoclimatic variability inferred from stable isotopes of planktonic foraminifers during marine isotope Stages (MIS) 1–5 with the Greenland ice core GISP2 record and thus establish the links between marine and terrestrial records.

Additionally, this stratigraphy forms the paleoclimatic framework and precise age model for a number of paleoceanographic and paleoclimatic studies published in this volume (**Tamburini et al., Boulay et al.**) and elsewhere (Higginson et al., 2003).

METHODS

Stable Isotope Analysis

The oxygen isotope record is based on *Globigerinoides ruber*, a near-surface-dwelling planktonic foraminifer (Bé and Tolderlund, 1971) that records changes in surface water $\delta^{18}O$ and $\delta^{13}C$ (Linsley and von Breymann, 1991). Stable oxygen and carbon isotope analyses at Site 1144 were made on 1667 samples at uneven sampling intervals (Table T1).

Approximately 15–20 cm³ of wet bulk sediment was freeze-dried, weighed, and wet-sieved to remove the <63-µm fraction. The sand fraction (>63 µm) was oven dried at 40°C for 24 hr and then weighed to determine the percent sand fraction.

Because foraminifer tests are rare in the common size class 315–400 µm, we chose to use the 250- to 315-µm fraction (Linsley and Dunbar, 1994; Lee et al., 1999). For each sample, ~15–20 tests of the planktonic foraminifer *G. ruber* (white) variety, were selected following the morphotype classification of Wang (2000).

F1. Leg 184 site locations, p. 20.

T1. Average sampling resolution, p. 26.

C. Bühring et al.
Stable Isotope Stratigraphy, Site 1144

3

In a few samples, not enough specimens complying with the sensu stricto morphotype requirements were found. These samples were supplemented with as many sensu latu tests as necessary to reach the amount of carbonate (150–200 μg) required for reliable measurements. The number of specimens (15–20) and the rather narrow size fraction were chosen to minimize the influence of vital effects (Berger et al., 1978) and, moreover, to average out the signal noise linked to differential bioturbational mixing.

Only tests that were intact and without visible dissolution were selected. A substantial effort was made to avoid *G. ruber* (pink), which is generally isotopically lighter ($\delta^{18}O = \Delta 0.17‰$) (Thompson et al., 1979) than *G. ruber* (white). At Site 1144, *G. ruber* (pink) is either light pink throughout or, more often, the pigmentation is very weak and only the very first chambers are pink colored, which complicates identification.
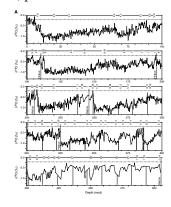
Before isotope analysis, the foraminifer tests of each sample were immersed in ultrapure ethanol, carefully cracked to expose the interior of the chambers, and ultrasonicated for 20 s. Subsequently, the ethanol, with possible contaminants still in suspension, was siphoned off with a syringe and the remaining foraminifer fragments were dried at 40°C. The cleaned samples for isotopic measurements weighed 150–200 μg. For isotope analysis, standard techniques were used: the carbonate was reacted with 100% orthophosphoric acid at 70°C, and the isotopic ratios were determined using a Finnigan MAT 251 micromass spectrometer with the Carbo Kiel device (Kiel I type) at the Leibniz Laboratory at Kiel University (Germany). Samples from the interval 172.16–182.17 meters composite depth (mcd) were measured on a Finnigan Delta Plus XL mass spectrometer combined with a Kiel GasBench II continuous flow interface. Precision was regularly checked by running (internal) Solnhofen limestone standards. Conversion to the Peedee belemnite (PDB) scale was performed using the National Bureau of Standards NBS-20 carbonate standard. For the MAT 251, the external standard errors over 1 yr (2000–2001) were <0.08‰ for $\delta^{18}O$ and <0.05‰ for $\delta^{13}C$ (both 1-σ values); on the Delta Plus XL mass spectrometer, the error reached <0.096‰ for $\delta^{18}O$ (NBS-19) and <0.06‰ for $\delta^{13}C$. The true uncertainty for *G. ruber* $\delta^{18}O$ data ranges from ±0.04‰ to ±0.08‰ on the basis of quasi-replicate analyses of centimeter-spaced samples from the Holocene section in neighboring SONNE-95 core 17940 (Wang et al., 1999a).

All stable isotope data for Site 1144 are given in the "Appendix," p. 19, and presented in Figure F2. Data are also available as an electronic file at www.pangaea.de/PangaVista.

Composite Depth Model

Instead of the meters below seafloor (mbsf) depth scale, we used the continuous shipboard (Shipboard Scientific Party, 2000) composite depth scale (mcd), which links sediment profiles of cores from Holes 1144A, 1144B, and 1144C to 235.41 mcd. Splicing of cores below this interval was precluded by incomplete core recovery and incidental alignment of core gaps (Shipboard Scientific Party, 2000). Although the cores below 235 mcd cannot be tied directly to the composite depth scale, the cores can be correlated with each other so that correlative features of multisensor track (MST) records and sediment color are matched in depth. This relative, or "floating," composite depth scale is not tied to the overlying composite depth scale (Shipboard Scientific Party, 2000). The majority of samples below 235 mcd are from Hole

F2. Oxygen and carbon isotope data, p. 21.

1144A; some gaps resulting from the floating composite depth scale were bridged with samples from Hole 1144B.

Radiocarbon-Based Age Control

Seventeen samples were radiocarbon dated to better constrain the age control of the Holocene to last glacial sediment section between 1.270 and 47.200 ka (see Table T2; Fig. F3). Five samples were dated on mixed bulk planktonic foraminifers (Chen and Shyu, unpubl. data), and twelve were dated on mixed planktonic *G. ruber* and *Globigerinoides sacculifer* (this study). The nine ^{14}C datings constrain ages between 1.27 and 40.95 ka. Note that most dates of MIS3 come close to the tuned ages of 20–50 ka, which were assigned to the core depths by simple correlation of the δ^{18}O record to the GISP2 record right below the top of Dansgaard-Oeschger (DO) Interstadial 2 (see "Appendix," p. 19; Figs. F2A, F3).

During the Last Glacial Maximum (LGM), the dates show an age reversal from 18.12 ka (^{14}C) at 14.97 mcd to 16.42 ka (^{14}C) at 17.22 mcd (see Table T2). In part, this reversal may stem from differences in the species analyzed. The lower sample consisted of specimens from *G. ruber* and *G. sacculifer,* which dwell in the surface layer with a modern ^{14}C reservoir age of ~465 a (Southon et al., 2002). In contrast, the upper sample consisted of mixed bulk planktonic foraminifers that possibly included specimens of species that dwell near and below the thermocline, where the ^{14}C reservoir age exceeds that of surface water by several hundred years (P.M. Grootes et al., unpubl. data). Moreover, local ^{14}C reservoir ages and their vertical gradient may have experienced significant short-term increases toward the end of the LGM, whereas primary ^{14}C production did not change significantly during this time (Hughen et al., 2004). Since these factors cannot yet be quantified, the precise origin of the age reversal remains unknown.

RESULTS AND DISCUSSION

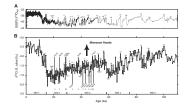## Oxygen Isotope Stratigraphy and Chronology: Overview

The 518-m-long sediment section reaches back to at least 1.03 Ma. Figure F3 shows the uppermost 120 m, spanning the last 140 k.y.

In general, the sawtooth-shaped δ^{18}O curve for Site 1144 records the 100-k.y. climatic cycles that are well established for the last 900 k.y. (Prell et al., 1986) (Figs. F2, F4). High-amplitude δ^{18}O variations occur throughout the entire Site 1144 record, with slightly decreasing amplitudes in the lowermost 100 m. The age model for Site 1144 was constructed by combining evidence from various reference records for age correlation. The uppermost 106 m of the Site 1144 δ^{18}O record was correlated to the δ^{18}O record of GISP2 (Grootes and Stuiver, 1997) and dated according to the GISP2 timescale (Alley et al., 1997; Meese et al., 1997) (Fig. F3). This correlation is largely supported by radiocarbon dates, although they show a slight age reversal near 15 mcd (see the "Appendix," p. 19; Figs. F2, F3).
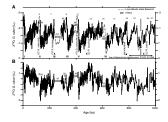
In the interval 110–504 mcd, MIS 5.52–29 (128–1027 ka) (Emiliani, 1955; Shackleton and Opdyke, 1973) were identified by visual correlation to orbitally tuned δ^{18}O records of ODP Site 658 (Sarnthein and

T2. AMS-^{14}C dates, p. 27.

F3. Oxygen isotope and planktonic δ^{18}O record, p. 23.

F4. Foraminiferal oxygen and carbon isotope data, p. 24.

Tiedemann, 1990), ODP Site 677 (Shackleton et al., 1990, 2002), and Marion Dufresne core MD90-0963 (Bassinot et al., 1994) (Figs. F2, F4). Ages for the whole record were defined through linear interpolation between the tie points listed in Table T2.

Below 480 mcd, age control was based on two biostratigraphic datums. MIS 31 (Figs. F2, F4) was used as a tie point to constrain the age of the upper end of the small *Gephyrocapsa* acme Zone (Gartner, 1988) at 500.66 mcd to 1100 ka (Tables T3, T4) (compared to 1020 ka, according to Shipboard Scientific Party, 2000). A major hiatus between 503.76 and 506.82 mcd is inferred from the last occurrence (LO) of *Discoaster brouweri/triradiatus* at 506.82 mcd (1960 ka, according to Shipboard Scientific Party, 2000). The isotope stage below the hiatus is possibly MIS 73 but cannot be identified with certainty.

Detailed Features in the Oxygen Isotope Record

Holocene

The Site 1144 Holocene $\delta^{18}O$ record displays a high-amplitude internal variability reaching 0.6‰–0.8‰ (Fig. F3). The lightest values of –2.85‰ were measured at 5.8 mcd (near 10 ka). They may stem from a freshwater plume near the Pearl River mouth that resulted from high precipitation and runoff from China (Wang et al., 1999a, 1999b, 1999c). In general, the Holocene oxygen isotope curve is similar to the $\delta^{18}O$ record of neighboring core 17940 reported in Wang et al. (1999a). An early suspicion that the uppermost 2 m of sediment may be lost at Site 1144 (Shipboard Scientific Party, 2000) seems disproved by the ^{14}C age of 1.7 ka (1.272 ± 0.060 k.y.) at 0.74 mcd. This is the approximate age expected for this core depth when taking into account the average Holocene sedimentation rate of ~0.5 m/k.y. at Site 1144. However, a small portion of the topmost sediment, we estimate ~7 cm, is still missing, since the oxidized reddish sediment surface was not recovered.

The planktonic Holocene to LGM $\delta^{18}O$ shift amounts to approximately Δ1.8‰, with maximum differences of 2.4‰ between short-term extremes in the Holocene and LGM. The ice volume effect on the $\delta^{18}O$ record for the most recent glacial–interglacial transition (MIS 1–2) is estimated to be 1.2‰, assuming that 10 m of sea level rise is equivalent to 0.11‰ change in $\delta^{18}O$ (Labeyrie et al., 1987; Fairbanks, 1989). Thus, the overall glacial–interglacial $\delta^{18}O$ shift at Site 1144 primarily records the global ice volume signal; in addition, fluctuations in local surface water temperature and/or salinity account for >0.6‰.

The Younger Dryas (YD) event (6.5–8.1 mcd) is recorded as a prominent isotopic shift of Δ0.7‰ back to more positive $\delta^{18}O$ values (Figs. F2A, F3) and shows the characteristic double-peak structure also known from the Greenland ice core records (Alley et al., 1993). Prior to the YD, a distinct $\delta^{18}O$ minimum near –2‰ marks the Bølling/Allerød warm phase (8.1–10.2 mcd). The top of MIS 2 is assigned to the major $\delta^{18}O$ shift of Δ0.8‰ toward the Bølling/Allerød level near 10.4 mcd (Termination IA).

Marine Isotope Stages 2–5

MIS 2–5 in the Site 1144 $\delta^{18}O$ record (Figs. F2A, F3) are characterized by frequent narrow-standing negative oscillations that reach Δ0.7‰– 0.85‰ in MIS 2 and 3, up to Δ0.9‰ in MIS 4, and Δ1.1‰ in late MIS

T3. Marine isotope data, p. 28.

T4. Biostratigraphic datums and age markers, p. 29.

5. These short-term $\delta^{18}O$ excursions are not analytical noise but instead form a reliable record of true climate change because

1. They exceed the analytical error by almost an order of magnitude;
2. Most spikes are not one-point peaks but are replicated by various data points at their peaks and/or along the flanks;
3. The given sampling space of 20–30 cm, equal to 200–300 yr, provides sufficient resolution for storing short-term differential climate signals in the sediment record; and
4. The tuned age correlation of the $\delta^{18}O$ oscillations between 20 and 41 ka was clearly confirmed by several calibrated ^{14}C ages within the error range of calibration (see the "Appendix," p. 19; Fig. F3).

In Figure F3 we correlated the most prominent positive $\delta^{18}O$ excursions in the uppermost 110 mcd of Site 1144 to North Atlantic Heinrich events 1–6 (H1–H6). On the other hand, the negative $\delta^{18}O$ excursions were correlated with DO interstadials (IS) in the $\delta^{18}O$ record of core GISP2 (sensu Schulz et al., 1998; Wang et al., 1999a). Accordingly, the analogs of IS events 3–7, 9–16, and 20–23 are well represented in the Site 1144 $\delta^{18}O$ record as prominent negative excursions. Their internal structure appears slightly more rugged than the IS in the GISP2 record.

Starting from the top of MIS 2 (10.45 mcd), the first major negative $\delta^{18}O$ excursion occurs between 16.9 and 19.0 mcd and was termed "20k IS" because it corresponds to a highly similar (yet unnamed) $\delta^{18}O$ excursion near 20 ka in the GISP2 record. The broad negative $\delta^{18}O$ interval between 23.9 and 26.4 mcd was correlated to IS 2 of core GISP2 near 23 ka, although it lacks the high negative spikes that mark the ice core record. However, bracketing ^{14}C datings (equal to 22.17 and 25.8 ka) (Fig. F3; see the "Appendix," p. 19) and the preceding strongly positive $\delta^{18}O$ excursions near 26.89 mcd, which correspond to H2, strongly support this interpretation. Similar to core GISP2, the analog to IS 8 at Site 1144 covers a broad bipartite interval but lacks the typical sawtooth pattern, perhaps because of still insufficient sampling resolution (267 yr). DO IS 10 is directly supported by a calibrated ^{14}C date of 40.05 ka (see the "Appendix," p. 19). The shape of the DO IS 16–17 equivalents at Site 1144 slightly differs from GISP2, but the $\delta^{18}O$ drastic increase below 66 mcd is a clear counterpart to the top of event H6 and marks the bottom of IS 17 at the top of MIS 4 (Fig. F3). Here, the structure between IS 18 and 19 is richer than in core GISP2. The bipartite IS 19 in core GISP2 was correlated to the broad, deeply structured interval from 73.5 to 78.8 mcd. The rugged equivalents of IS 21, 22, and 23 at Site 1144 represent marine isotope Substages 5.1, 5.3.1, and 5.3.3, respectively.

The H3 event is weak in comparison to its equivalent in core GISP2; it is, however, well confirmed by a calibrated ^{14}C age of 30.72 ka (Sarnthein et al., 2000) at 33.07 mcd. Farther downcore, the prominent positive $\delta^{18}O$ excursion at 44.5 mcd corresponds to event H4 (see the "Appendix," p. 19; Fig. F3). The H5 equivalent at 53.6 mcd has a proper calibrated ^{14}C age of –47 ka, but the broad sawtooth structure of $\delta^{18}O$ minima farther below, including IS 14, clearly matches the pertinent $\delta^{18}O$ record of IS 14 in core GISP2. A pronounced increase in $\delta^{18}O$ close to 61 mcd is tentatively assigned to Heinrich subevent 5.2 (van Kreveld et al., 2000; Sarnthein et al, 2000).

Only the very top of MIS 5.5 and the MIS 5.4–5.5 transition are preserved downcore from MIS 5.4 (centered around 107 mcd; ~108 ka) subsequent to ~116 ka (Figs. F2A, F4). Most of MIS 5.5 is missing according to the stratigraphic definition of Shackleton et al. (2002). This major hiatus, spanning ~12 k.y., is deduced from an obvious lack of sediment thickness and, in particular, from the fact that the $\delta^{18}O$ minimum of approximately –2.5‰ misses by far the negative extreme of –2.9‰/–3.2‰ characteristic of MIS 5.51 in other cores from this region (Linsley, 1996: ODP Hole 769A; Wang et al., 1999a: SONNE-95 core 17954; Lee et al., 1999: Marion Dufresne core MD972151) and at neighboring Site 1145 (Oppo and McIntyre, unpubl. data; McIntyre and Oppo, 2001). The hiatus is also documented by the LO of *G. ruber* (pink). It lies at the top of a pronounced positive $\delta^{18}O$ excursion at 110–111 mcd, whereas it has been generally established for the top of an extreme $\delta^{18}O$ minimum indicating MIS 5.51 (116 ka). Finally, the hiatus at 110 mcd corresponds to an abrupt $\delta^{13}C$ shift of more than $\Delta 0.5$‰ (Figs. F2B, F4B). Farther downcore, the $\delta^{13}C$ record shows a broad extreme minimum similar to that observed for late MIS 6 at Atlantic ODP Site 658 (Sarnthein and Tiedemann, 1990).

Below the hiatus, the short-term positive $\delta^{18}O$ excursion near 110–111 mcd most likely represents a YD-style climatic oscillation (event 5.52 or H11 at >128 ka) (Sarnthein and Tiedemann, 1990; Shackleton et al., 2002). The preceding negative peak is assigned to warm event 5.53 near 130 ka. The transition from MIS 6 to MIS 5.53 (Termination II) near 113 mcd reveals an almost instantaneous $\delta^{18}O$ shift of 1.25‰ (Figs. F2A, F4A).

The millennial- to submillennial-scale variations in the planktonic stable isotope record of MIS 2–5 at Site 1144 match the high-resolution sea-surface salinity record of neighboring core 17940 (back to DO IS 9) (Wang et al., 1999a) and the $\delta^{18}O$ record of SONNE-95 core 17924 (150 km farther east; M. Sarnthein, unpubl. data). Thus the short-term $\delta^{18}O$ changes at Site 1144 can be interpreted as large-scale changes in sea-surface salinity in addition to minor changes in sea-surface temperature and global ice volume (Lambeck and Chappell, 2001). Because of the close vicinity to the Pearl River mouth, the short-lasting freshwater pulses at Site 1144 especially record short increases in fluvial runoff induced by enhanced precipitation and summer monsoon intensity on the Chinese mainland. On the other hand, any decrease in summer monsoon intensity has resulted in decreased precipitation and/or in sea-surface temperature reduction at Site 1144. Thus the short-term maxima in planktonic $\delta^{18}O$ provide a record of high salinity off South China during major and minor stadials.

The question is not fully answered yet (An, 2000) as to whether sudden $\delta^{18}O$ variations in the SCS were precisely coeval with the DO interstadial and stadial events in the North Atlantic and the Greenland Ice Sheet (Dansgaard et al., 1993; Adkins et al., 1997; Bond et al., 1997; van Kreveld et al., 2000). However, we regard it as most likely that the short-term changes in Asian Monsoon intensity were intimately tied to high-latitude climate forcing via atmospheric signal transfer (Wang et al., 1999b; Kudrass et al., 2001). This concept is corroborated by recent U/Th datings of a speleothem record in China (Wang et al., 2001) and a model study of Mikolajewicz et al. (1997). They showed that atmospheric transfer of Greenland temperature variations would have resulted in quasisynchronous signals across the entire Northern Hemisphere.

In contrast to a scenario in which the SCS was primarily responding to climate changes in northern high latitudes, an opposite scenario may be considered, in which tropical climate and the monsoon system were the driving forces for Northern Hemisphere millennial-scale climate variations. Recent models of Clement and Cane (1999) and Clement et al. (1999) indeed suggest that long-term oscillations of the El Niño–Southern Oscillation may have been an important forcing factor for millennial-scale changes in the climate system of tropical monsoon and, furthermore, may have exerted an important influence on global climate change.

Marine Isotope Stages 6–11

Below the hiatus at MIS 5.5, the δ^{18}O record of marine isotope Stage 6 shows well-developed Substages 6.2–6.6 (Figs. F2, F4) as in various other records from the South China and Sulu Seas (Linsley and Dunbar, 1994; Wang et al., 1999a). Moreover, there are ongoing millennial-scale oscillations with internal amplitude variations reaching $\Delta1.0‰$, similar to (possibly coeval?) δ^{18}O oscillations at neighboring Site 1145 (Oppo and McIntyre, unpubl. data) and the short-term variations in MIS 3–4.

The precise stratigraphic assignment of MIS 6.5 and the MIS 6/7 boundary (~190 ka) were subject to extensive discussion among the Leg 184 shipboard scientific party because of planktonic δ^{18}O values for MIS 6.5, which are as negative as those in MIS 7.1. Final correlations were established by means of (1) a benthic δ^{18}O record for the interval 153–185 mcd, which shows a massive δ^{18}O increase by more than $\Delta1.0‰$ near 175 mcd to be used as stage boundary (Clemens et al., unpubl. data); and (2) a precise correlation of the Site 1144 planktonic δ^{18}O record with that of neighboring Site 1145 (Oppo and McIntyre, unpubl. data).

Planktonic δ^{18}O values of MIS 7.1 and 7.3 do not quite reach the interglacial level of the Holocene (–2.6‰), only the values of MIS 7.5 near 234 ka, a trend similar to that of other δ^{18}O records from this sea region (Linsley and von Breymann, 1991; Wang et al., 1999a). Sedimentation rates in warm MIS 7 are clearly reduced compared to MIS 6 (Table T2). The amplitude of cold Substage 7.4 (221 ka) (Figs. F2A, F4) is similar to that at Site 1145 (Oppo and McIntyre, unpubl. data) but appears less "glacial" than in SPECMAP (Martinson et al., 1987) and Site 769 isotope curves.

The detailed and accurate fit of the planktonic δ^{18}O curves from Sites 1144 and 1145 (Oppo and McIntyre, unpubl. data) also led to the definition of a major hiatus reaching from the top of MIS 7.5 down to the lower top of MIS 8.5 at Site 1144. Like the stratigraphic gap at peak MIS 5.51, the erosional event near MIS 7.5 appears linked to peak interglacial conditions. Unlike MIS 5.5, erosion had ended shortly before the peak interglacial during late glacial Termination III and deleted the complete antecedent glacial sediment section.

Unlike various stratigraphic reference curves (Bassinot et al., 1994) MIS 9.1 is broad and bipartite in the δ^{18}O records of Sites 1144 and 1145 (307–313 ka) (Figs. F2, F4) (Oppo and McIntyre, unpubl. data). Two warm Substages 9.11 and 9.13 are clearly detached by a δ^{18}O increase of $\Delta1.3‰$, identified as cold Substage 9.12. Below, δ^{18}O values reach the Holocene δ^{18}O level in warm MIS 9.3, which is separated from MIS 9.1 by a positive 1‰ excursion in MIS 9.2. A major δ^{18}O shift of 1.5‰ constitutes the MIS 9/10 boundary (Termination IV) at 208 mcd (334 ka)

(Figs. F2A, F4). Oxygen isotope values for antecedent cold MIS 10.2 (up to –0.5‰) are slightly higher than for MIS 2. High-frequency $\delta^{18}O$ variations during MIS 10.2–11.1 reach Δ1‰, similar to the $\delta^{18}O$ amplitudes of DO cycles in MIS 2–4.

Despite sufficient sampling resolution, most of the characteristically broad interglacial MIS 11.3 is missing (Figs. F2, F4), similar to the stratigraphic gaps outlined for peak interglacials MIS 5.5 and 7.5. This gap is also suggested by minimum isotope values of –2.5‰ that are far more positive than the values of –3.1‰ recorded at neighboring Site 1145 (Oppo and McIntyre, unpubl. data). Based on detailed comparison with other planktonic high-resolution records of MIS 11.3 (Berger et al., 1993a, 1993b; McManus et al., 1999), we place the major hiatus somewhere between 246.33 and 247.13 mcd (~413–397 ka) (Figs. F2A, F4), comprising ~15 k.y. Similar to the base of the hiatus in Stage 5.5, the base of this hiatus lies within a YD-style cold episode right after the short warm event 11.33 (sensu Sarnthein and Tiedemann, 1990), which is comparable to the Bølling/Allerød warm phase at the end of the last glacial.

Marine Isotope Stages 12–25

MIS 12 (250–289 mcd; 423–471 ka) (Fig. F2A, F4) is the most prominent glacial of the last 800 k.y., with average $\delta^{18}O$ values as much as 0.4‰ heavier than during MIS 2. The $\delta^{18}O$ record separates three major cold events (MIS 12.22, 12.24, and 12.4) and numerous short-term climatic oscillations similar to those found in MIS 2–4.

MIS 13 and 15 do not display the characteristic trident shape expected on the basis of the stratigraphic reference record of Bassinot et al. (1994). The $\delta^{18}O$ record of MIS 13 and 14 may be complete. On the other hand, we strongly surmise that MIS 15 has lost peak interglacial Substage 15.5 near 610 ka, similar to the hiatuses found at peak interglacial Substages 11.3, 7.5, and 5.51. In Figure F2 we placed the hiatus to the $\delta^{18}O$ jump at 325 mcd. This postulation receives independent support from an abrupt major drop in sedimentation rates by a factor of 4 for lower MIS 15, if no hiatus is assumed (Fig. F5).

Peak glacial MIS 16 (623–650 ka) is broadly developed, consisting of Substages 16.2 and 16.4 with average $\delta^{18}O$ values as high as those during MIS 2. MIS 17 is clearly tripartite and MIS 18 is bipartite with a broad Substage 18.3, as in the reference record of Bassinot et al. (1994). This general coherency of records also applies to MIS 19–21. A layer of Australasian microtektites (Zhao, unpubl. data) provides an important age marker within the lower part of the MIS 19–20 transition at 386.2 ± 0.03 mcd, right below the Brunhes/Matuyama boundary.
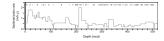
Narrow-standing isotope Stages 22–33 were identified through comparison with $\delta^{18}O$ records of ODP Sites 607, 677, and 659 (Tiedemann et al., 1994), where MIS 27 turns out to be clearly bipartite.

Millennial-scale climate variability over MIS 13–19 shows $\delta^{18}O$ amplitudes of 0.6‰–0.9‰, which are as high as those in MIS 2–4 and other Pleistocene stages (Fig. F2A).

Marine Isotope Stages 26–(?)34 and Features near the Base of the Core Profile

Below 422 mcd (~970 ka), sampling intervals still range between 1.5 and 2 m (Figs. F2, F4). Thus, MIS 26–33 are assigned only tentatively

F5. Sedimentation rates, Site 1144, p. 25.

but bear the potential for a high-resolution climatic record because of high sedimentation rates (Fig. F5).

A major hiatus, deduced from biostratigraphy (Shipboard Scientific Party, 2000), occurs below MIS 33 (Figs. F2A, F4), which, accordingly, may be incomplete. Based on two biostratigraphic ages (Tables T3, T4), the hiatus spans almost 0.85 m.y. Farther downcore a definitive designation of isotope stages for the interval 509.3–517.9 mcd was not possible. The LO of *D. brouweri/triradiatus* (1.96 Ma) possibly represents MIS 73 (Sarnthein and Tiedemann, 1989) at 506.82 mcd. Assuming a constant average sedimentation rate of 0.50 m/k.y., the lowermost depth at Site 1144 (517.56 mcd) may reach an age of 1.982 Ma (Tables T3, T4).

Sedimentation Rates

Site 1144 is located on a thick sediment drift (Sarnthein et al., 1994; Shipboard Scientific Party, 2000) where changes in sedimentation rate mainly reflect variations in downslope terrestrial input and/or lateral reworking and transport by bottom current activity. Accordingly, Site 1144 is characterized by generally high sedimentation rates (Table T2; Fig. F5). From 507 to 100 mcd (MIS 33 to MIS 6 top) linearly interpolated sedimentation rates vary between 0.2 and 0.9 m/k.y. Higher rates mark glacial MIS 20, 18.4, 16, and, especially, MIS 10 and 6.6; lower rates mark interglacial sediment sections.

This trend culminates in hiatuses during peak interglacial MIS 15.3, 11.3, 9.1, lower MIS 7.5, and MIS 5.5, where the $\delta^{18}O$ minima neither reach a level analogous to the Holocene nor cover sediment sections that are as thick as those in the Holocene section (Figs. F2, F4). Thus, major portions of the interglacial sediment sections appear to be lost in major and minor stratigraphic gaps as also revealed by direct comparison with $\delta^{18}O$ records of neighboring Sites 1144 and 1145 (S. Clemens and M. Sarnthein, pers. corr., 2002). A similar sediment loss may also apply to MIS 9.3, where the linearly interpolated sedimentation rate decreases to a rare low of 0.15 m/k.y. and may contain short stratigraphic gaps. Most hiatuses correspond to minor or major unconformities in the seismic record at Site 1144 (Shipboard Scientific Party, 2000).

We tend to ascribe the striking stratigraphic gaps to shifts in the intensity and/or vertical shifts in the axis of a deep boundary current, the incursion of Pacific Intermediate Water. The current shifts were probably linked to changes in global thermohaline circulation characteristic of early to peak interglacial stages. Indeed, Sarnthein et al. (1994) and Lehmann (1996) found a pertinent PARASOUND echo character, erosional microfurrows that today are widespread and form a record of modern strong bottom current action at water depths *below* Site 1144.

From 100 mcd to near the sediment surface, sedimentation rates gradually increase from 0.5 to 1.8 m/k.y. (Fig. F5). This increase may be apparent, partly as a result of still modest sediment compaction and higher water contents (Shipboard Scientific Party, 2000), and partly because maximum sedimentation rates are tied to peak glacial MIS 4 and 2, similar to the maxima of glacial stages farther downcore.

Note that the high maximum sedimentation rates in MIS 2 contrast with the rates found at neighboring site 17940 farther upslope (Wang et al., 1999a). At site 17940, maximum rates of ~0.7 m/k.y. mark the Preboreal and early Holocene section, whereas glacial sedimentation rates drop to 0.2 m/k.y. during MIS 2–3. This difference in the trend of sedimentation rates (1) may be an artifact near the core top of the two sites, resulting from different coring techniques, or (2) may stem from the

slightly greater water depth at Site 1144 (Fig. F1), which was subject to enhanced deposition when the glacial sea level reached a minimum. Lüdmann et al. (2001) suggested that differences in sedimentation rates may be linked to complex interactions between sea level stand and the location of maximum sediment discharge from the Pearl River mouth. They surmise that the synglacial exposure of the Dongsha Island area, northwest of Site 1144, led to a deviation of the sediment plume from east to west of the island group during the LGM and back to east when the shelf again was flooded during the early Holocene. In this way, the deeper Site 1144 would possibly receive much more hemipelagic sediment during times of low sea level, whereas site 17940, ~300 m farther upslope, would receive more sediment during sea level high stands.

Carbon Isotope Record

Glacial–interglacial variations in planktonic $\delta^{13}C$ at Site 1144 reach $\Delta0.6‰–1.1‰$ over the past 1.1 m.y. These variations form a record of changes in the composition of dissolved inorganic carbon (DIC), which in turn depends on the nutrient concentration and the isotopic composition of dissolved atmospheric CO_2 and CH_4 near the sea surface (~30 m water depth). Long-term $\delta^{13}C$ changes roughly parallel the general climate cyclicity of the last 1 m.y. and are dominated by the ~100-k.y. eccentricity cycle.

High $\delta^{13}C$ levels were more common during (late) warm $\delta^{18}O$ stages and interstadials. However, very high $\delta^{13}C$ values also marked early glacial MIS 2, semiglacial MIS 3, and large parts of MIS 12–13, where $\delta^{13}C$ values reached or approached the late Holocene level of 1.2‰–1.4‰. Over longer times, maximum $\delta^{13}C$ values culminated at ~30 (MIS 2/3 boundary), ~480 (MIS 13.1), and ~1035 ka (top MIS 31) (see the "Appendix," p. 19; Figs. F2B, F4B) and thus formed a sort of overlying 450-k.y. cycle possibly controlled by orbital eccentricity.

On the other hand, minimum $\delta^{13}C$ values of 0.0‰–0.25‰ were most common near the end of each peak glacial stage and the subsequent glacial Terminations I, II, IV, and V. Similar $\delta^{13}C$ minima also marked the glacial terminations leading from MIS 7.4 to 7.3, MIS 18.4 to 18.3, and, especially, MIS 22 to 21. Further potential $\delta^{13}C$ minima at Terminations III and VI were lost in the hiatuses outlined above. In addition, there was a $\delta^{13}C$ minimum at early MIS 16. Immediately after the $\delta^{13}C$ minimum at each glacial termination, we find the largest shifts in $\delta^{13}C$ ($\Delta1.1‰$) (Figs. F2B, F4B). Some $\delta^{13}C$ gradients are spurious since they were steepened by hiatuses, in particular after glacial Stages 2, 6, 10, and 12.

The younger portion of the planktonic $\delta^{13}C$ record at Site 1144 (Figs. F2B, F4B) is consistent with records from neighboring core 17940 and various other SONNE-95 cores from the SCS (Wang et al., 1999a). Moreover, the major $\delta^{13}C$ minima (Figs. F2B, F4B) are consistent with deglacial minima found in many other low-latitude planktonic records (Linsley and Dunbar, 1994; Oppo and Fairbanks, 1989), in the subarctic North Pacific (M. Sarnthein, unpubl. data), and many Atlantic $\delta^{13}C$ records (Tiedemann, 1994). Thus, the long-term overall $\delta^{13}C$ reduction along Pleistocene glacial terminations may in part represent a global feature.

In part, the minima in $\delta^{13}C$ toward the end of the glacial maxima and early interglacial times may also result from local factors such as short-term enhanced riverine nutrient input (Wang et al., 1999a), trig-

gering high productivity and enriching remineralized organic carbon and ^{12}C in nearshore surface water. During Termination I, the switch back to high $\delta^{13}C$ values only occurred after the Preboreal, when a prominent maximum in local freshwater and nutrient input had ended and/or shifted landward on the inundated shelf as a result of ongoing sea level rise. This freshwater plume is clearly recorded as massive sea-surface salinity reduction in neighboring core 17940 during the Preboreal (Wang et al., 1999b) and documents a maximum in summer monsoon precipitation over China. This conclusion is corroborated by a short-term culmination in clay accumulation rates, probably the result of prominent sediment discharge from the Pearl River (Wang et al., 1999a).

Refined Age Control of Biostratigraphic and Other Datums

To refine the age assignment of Pleistocene biostratigraphic datums (Table T3) and the Australasian microtektite layer in the SCS, we employed the age model of Table T2, which in turn is tuned to the astronomical timescale developed for the stacked $\delta^{18}O$ records of ODP Site 677 and core MD90-0963 by Bassinot et al. (1994). This approach was partially successful; it was hampered by frequent stratigraphic gaps in the Site 1144 sediment section.

The latter problem applies to the LO of *G. ruber* (pink) at Site 1144 at 110.30 mcd. Since this depth forms the base of a hiatus across Interglacial Stage 5.5, the actual LO position lies within the lost sediment section, somewhere between 128 and 116 ka (Table T2; Fig. F2A, F4A).

The first occurrence (FO) of *Emiliania huxleyi* was found at 192.82 mcd (Shipboard Scientific Party, 2000), which corresponds to the middle of MIS 7.4 with an assigned age of ~227 ka. Because of the 50-k.y. hiatus at Site 1144 below MIS 7.5, this FO age is much younger than the ages generally assigned to the FO of *E. huxleyi* within MIS 8.4–8.5 at 268 to 285 ± 3.5 ka (Thierstein et al., 1977; Vergnaud Grazzini et al., 1990; Ahagon et al., 1993).

The number of *G. ruber* (pink) used for defining the *G. ruber* (pink) acme Zone increases abruptly just above MIS 11.3 in the Site 1144 $\delta^{18}O$ record at 248.39 mcd (417 ka). By contrast, the Shipboard Scientific Party (2000) described this prominent increase in *G. ruber* (pink) farther upcore, at 261 mcd (400 ka) (Li, 1997). However, specimens of *G. ruber* (pink) also occur farther downcore to 273 mcd (early MIS 12; 470 ka) and increase in several deeper samples, although the coloration of these specimens is very faint and mostly restricted to juvenile chambers. A similar gradual increase was first reported by Thompson et al. (1979) from the western equatorial Pacific. The clearly recognizable increase in frequency and coloration of *G. ruber* at 248.39 mcd may also reflect an improved preservation of the pigment (Thompson et al., 1979). In summary, we propose a new age of 417 ka for the onset of the *G. ruber* (pink) acme Zone in the SCS, an age that is slightly older than that generally reported for sediment records of the low-latitude West Pacific.

The LO of *Pseudoemiliania lacunosa* lies close to the MIS 12/13 boundary at 288.54 mcd (Shipboard Scientific Party, 2000), which corresponds to an age of 493 ka (Table T2). This date clearly precedes the dates defined through $\delta^{18}O$ records of cores V28-238 and 239 (Shackleton and Opdyke, 1973), where *P. lacunosa* only becomes extinct in MIS 12.4 (Thierstein et al., 1977).

The Brunhes/Matuyama boundary was not identified at Site 1144 by the Leg 184 Shipboard Party. Subsequent shore-based paleomagnetic measurements (Solheid et al., this volume) have neither confirmed the shipboard results (Shipboard Scientific Party, 2000) nor furnished new evidence of the most important paleomagnetic events. Instead, we used a layer of Australasian microtektites at 386.18–386.23 mcd, centered at ~386.21 mcd (Zhao, unpubl. data) as an independent age marker to establish solid age control for the MIS stratigraphy of Site 1144 near the Brunhes/Matuyama boundary. Published $^{40}Ar/^{39}Ar$ ages of the Australasian microtektites range from 783 ± 21 ka (Izett and Obradovich, 1992) and 784 ± 12 ka (Kunz et al., 1995) to 761 ± 17 ka and 816 ± 7 ka (Yamei et al., 2000). The microtektite layer was also found in SONNE-95 sediment core 17957 from the southern SCS (Jian et al., 2000; Zhao et al., 1999) where the abundance of microtektites culminates within the MIS 19–20 transition, 10 cm (~11.6 k.y.) below the Brunhes/Matuyama reversal (Wang et al., 2000). At Site 1144 the microtektite layer also lies within the lower MIS 19–20 transition. On the basis of our age model (Table T2), the layer has an age of 787 ka, similar to the age of 793 ka reported by Lee and Wei (2000).

The LO of *Reticulofenestra asanoi* occurs in the Site 1144 sediment profile at 417.23 mcd within MIS 24, which is slightly deeper than the definition of Wei (1993) (MIS 22–23) and leads to an assigned age of 912 ka.

CONCLUSIONS

The oxygen and carbon isotope stratigraphies for Site 1144 were obtained from hemipelagic sediments collected from the northern continental slope of the SCS. The isotopic record covers a >500-m-long sediment profile spanning the last 1.1 m.y. from the early Pleistocene to the Holocene. The intense hemipelagic deposition is probably linked to both lateral advection of terrigenous sediments in the nepheloid layer and oscillating boundary current activity, leading to a thick drift-type deposit. On the basis of outstandingly high sedimentation rates near 50–100 cm/k.y., the sediment profile of Site 1144 provides a high-resolution record of stable isotope oscillations and monsoon history on orbital to centennial timescales over the last 1.1 m.y.

Our analysis of the Site 1144 $\delta^{18}O$ and $\delta^{13}C$ records led to the following conclusions:

1. Subsequent to MIS 27 (950 ka), the long-term paleoclimatic record is largely dominated by standard sawtooth pattern 100-k.y. cycles.
2. Several major and minor hiatuses interrupt the sediment profile, tied to peak interglacial Stages 5.5, 7.5 (reaching back to MIS 8.5), 9.1, 11.3, and 15.5. These stratigraphic gaps are also reflected in the seismic record. They possibly result from an intensified contour current regime along the lower continental margin of South China, controlled by incursions of Upper Pacific Deep Water, which were enhanced near the end of major glacial terminations.
3. Pronounced millennial-scale cycles dominate the short-term $\delta^{18}O$ variability in monsoon intensity over the last 900 k.y. During the last 110 k.y., the cycles closely match the climate variability of DO cycles as documented in the GISP2 $\delta^{18}O$ record.

Similar high-frequency oscillations with comparable amplitudes in planktonic $\delta^{18}O$ are documented for MIS 6, lower 8–11, 12–15, and 16–24. Short-term climatic reversals similar to the YD are recorded within most glacial terminations, such as at the onset of warm MIS 5.5, 9.3, 11.3, and 19.

4. The planktonic carbon isotope record at Site 1144 shows long-term surface water $\delta^{13}C$ oscillations, which parallel the 100-k.y. eccentricity variations of the past 0.9 m.y. Moreover, $\delta^{13}C$ values form two 450-k.y. cycles culminating at ~30, ~480, and ~1035 ka. The variations in $\delta^{13}C$ are a global feature also seen in the North Atlantic and possibly result from oscillations in East Asian monsoon intensity, which controls local changes in wind stress and riverine nutrient supply and thus is responsible for the advection of nutrient-enriched surface water and/or the discharge of ^{13}C-depleted terrestrial organic carbon.

ACKNOWLEDGMENTS

REFERENCES

Adkins, J.F., Boyle, E.A., Keigwin, L.D., and Cortijo, E., 1997. Variability of the North Atlantic thermohaline circulation during the last interglacial period. *Nature,* 390:154–156.

Ahagon, N., Tanaka, Y., and Ujiie, H., 1993. *Florisphaera profunda,* a possible nanno-plankton indicator of late Quaternary changes in sea-water turbidity at the north-western margin of the Pacific. *Mar. Micropaleontol.,* 22:255–273.

Alley, R.B., Meese, D.A., Shuman, C.A., Gow, A.J., Taylor, K.C., Grootes, P.M., White, J.W.C., Ram, M., Waddington, E.D., Mayewski, P.A., and Zielinski, G.A., 1993. Abrupt increase in Greenland snow accumulation at the end of the Younger Dryas event. *Nature,* 362:527–529.

Alley, R.B., Shuman, C.A., Meese, D.A., Gow, A.J., Taylor, K.C., Cuffey, K.M., Fitz-patrick, J.J., Grootes, P.M., Zielinski, G.A., Ram, M., Spinelli, G., and Elder, B., 1997. Visual-stratigraphic dating of the GISP2 ice cores: basis, reproducibility and appli-cation. *J. Geophys. Res.,* 102:26367–26382.

An, Z., 2000. The history and variability of the east Asian paleomonsoon climate. *Quat. Sci. Rev.,* 19:171–187.

Bassinot, F.C., Labeyrie, L.D., Vincent, E., Quidelleur, X., Shackleton, N.J., and Lance-lot, Y., 1994. The astronomical theory of climate and the age of the Brunhes–Matu-yama magnetic reversal. *Earth Planet. Sci. Lett.,* 126:91–108.

Bé, A.W.H., and Tolderlund, D.S., 1971. Distribution and ecology of living planktonic foraminifera in surface waters of the Atlantic and Indian Oceans. *In* Funnel, B.M., and Riedel, W.R. (Eds.), *The Micropaleontology of Oceans:* Cambridge (Cambridge Univ. Press), 105–149.

Berger, W.H., Bickert, T., Schmidt, H., and Wefer, G., 1993a. Quaternary oxygen iso-tope record of pelagic foraminifers: Site 806, Ontong Java Plateau. *In* Berger, W.H., Kroenke, L.W., Mayer, L.A., et al., *Proc. ODP, Sci. Results,* 130: College Station, TX (Ocean Drilling Program), 381–395.

Berger, W.H., Bickert, T., Schmidt, H., Wefer, G., and Yasuda, M., 1993b. Quaternary oxygen isotope record of pelagic foraminifers: Site 805, Ontong Java Plateau. *In* Berger, W.H., Kroenke, L.W., Mayer, L.A., et al., *Proc. ODP, Sci. Results,* 130: College Station, TX (Ocean Drilling Program), 363–379.

Berger, W.H., Diester-Haass, L., and Killingley, J.S., 1978. Upwelling off Northwest Africa: the Holocene decrease as seen in carbon isotopes and sedimentological indicators. *Oceanol. Acta,* 1:1–7.

Bond, G., Showers, W., Cheseby, M., Lotti, R., Almasi, P., deMenocal, P., Priore, P., Cullen, H., Hajdas, I., and Bonani, G., 1997. A pervasive millenial-scale cycle in North Atlantic Holocene and glacial climates. *Science,* 278:1257–1266.

Clement, A.C., and Cane, M., 1999. A role for the tropical Pacific coupled ocean-atmosphere system on Milankovitch and millennial time scales. Part I. A modeling study of tropical Pacific variability. *In* Clark, P.U., Webb, R.S., and Keigwin, L.D. (Eds.), *Mechanisms of Global Climate Change at Millennial Time Scales.* Geophys. Monogr., 112:363–371.

Clement, A.C., Seager, R., and Cane, M.A., 1999. Orbital controls on the El Nino/ Southern Oscillation and the tropical climate. *Paleoceanography,* 14:441–456.

Dansgaard, W., Johnsen, S.J., Clausen, H.B., Dahl-Jensen, D., Gundestrup, N.S., Ham-mer, C.U., Hvidberg, C.S., Steffensen, J.P., Sveinbjörnsdottir, A.E., Jouzel, J., and Bond, G., 1993. Evidence for general instability of past climate from a 250-kyr ice-core record. *Nature,* 364:218–220.

Emiliani, C., 1955. Pleistocene temperatures. *J. Geol.,* 63:538–578.

Fairbanks, R.G., 1989. A 17,000-year glacio-eustatic sea level record: influence of gla-cial melting rates on the Younger Dryas event and deep-ocean circulation. *Nature,* 342:637–642.

Gartner, S., 1988. Paleoceanography of the Mid-Pleistocene. *Mar. Micropaleontol.,* 13:23–46.

Grootes, P.M., and Stuiver, M., 1997. Oxygen 18/16 variability in Greenland snow and ice with 10^{-3}- to 10^5-year resolution. *J. Geophys. Res.,* 102:26455–26470.

Higginson, M.J., Maxwell, J.R., and Altabet, M.A., 2003. Nitrogen isotope and chlorin paleoproductivity records from the northern South China Sea: remote vs. local forcing of millennial- and orbital-scale variability. *In* Clemens, S.C., Wang, P., and Prell, W.L. (Eds.), *Asian Monsoons and Global Linkages on Milankovitch and Sub-Milankovitch Time Scales.* Mar. Geol., 201:223–250.

Hughen, K., Lehman, S., Southon, J., Overpeck, J., Marchal, O., Herring, C., and Turnbull, J., 2004. ^{14}C activity and global carbon cycle changes over the past 50,000 years. *Science,* 303:202–207.

Izett, G.A., and Obradovich, J.D., 1992. Laser-fusion ^{40}Ar-^{39}Ar ages of Australasian tektite cores and flanges. *Eos, Trans. Am. Geophys. Union,* 73:328.

Jian, Z., Wang, P., Chen, M.-P., Li, B., Zhao, Q., Bühring, C., Laj, C., Lin, H.-L., Pflaumann, U., Bian, Y., Wang, R., and Cheng, X., 2000. Foraminiferal responses to major Pleistocene paleoceanographic changes in the southern South China Sea. *Paleoceanography,* 15:229–243.

Kudrass, H.R., Hofmann, A., Doose, H., Emeis, K., and Erlenkeuser, H., 2001. Modulation and amplification of climatic changes in the Northern Hemisphere by the Indian summer monsoon during the past 80 k.y. *Geology,* 29:63–66.

Kunz, J., Bollinger, K., Jessberger, E.K., and Storzer, D., 1995. Ages of Australasian tektites. In *Abstracts of papers submitted to the Twenty-sixth Lunar and Planetary Science Conference:* Houston, TX (Lunar and Planetary Inst.), 809–810.

Labeyrie, L.D., Duplessy, J.C., and Blanc, P.L., 1987. Variations in mode of formation and temperature of oceanic deep waters over the past 125,000 years. *Nature,* 327:477–482.

Lambeck, K., and Chappell, J., 2001. Sea level change through the last glacial cycle. *Science,* 292:679–686.

Lee, M.-Y., Wei, K.-Y., and Chen, Y.-G., 1999. High resolution oxygen isotope stratigraphy for the last 150,000 years in the southern South China Sea: core MD972151. *Terr. Atmos. Oceanic Sci.,* 10:239–254.

Lee, M.-Y., and Wei, K.-Y., 2000. Australasian microtektites in the South China Sea and West Philippine Sea: implications for age, size and location of the impact crater. *Meteorit. Planet. Sci.,* 35:1151–1155.

Lehmann, A., 1996. Sedimentation und Erosion am Kontinentalhang von Südchina [diploma thesis]. Univ. Kiel, Germany.

Li, B., 1997. Paleoceanography of the Nansha area, southern South China Sea since the last 700,000 years [Ph.D. dissert.]. Nanjing Inst. Geol. Paleontol., Academic Sinica, Nanjing, China. (in Chinese, with English abstract)

Linsley, B.K., 1996. Oxygen-isotope record of sea level and climate variations in the Sulu Sea over the past 150,000 years. *Nature,* 380:234–237.

Linsley, B.K., and Dunbar, R.B., 1994. The late Pleistocene history of surface water δ^{13}C in the Sulu Sea: possible relationship to Pacific deepwater δ^{13}C changes. *Paleoceanography,* 9:317–340.

Linsley, B.K., and von Breymann, M.T., 1991. Stable isotopic and geochemical record in the Sulu Sea during the last 750 k.y.: assessment of surface water variability and paleoproductivity changes. *In* Silver, E.A., Rangin, C., von Breymann, M.T., et al., *Proc. ODP, Sci. Results,* 124: College Station, TX (Ocean Drilling Program), 379–398.

Lüdmann, T., Wong, H.K., and Wang, P., 2001. Plio–Quaternary sedimentation processes and neotectonics of the northern continental margin of the South China Sea. *Mar. Geol.,* 172:331–358.

Martinson, D.G., Pisias, N.G., Hays, J.D., Imbrie, J., Moore, T.C., Jr., and Shackleton, N.J., 1987. Age dating and the orbital theory of the ice ages: development of a high-resolution 0 to 300,000-year chronostratigraphy. *Quat. Res.,* 27:1–29.

McIntyre, K., and Oppo, D., 2001. South China Sea surface waters during the late Pleistocene: records of the relationship between south east Asian monsoon variability and glacial–interglacial cycles [AGU Spring Meeting, Boston, 29 May–2 June, 2001]. (Abstract)

McManus, J.F., Oppo, D.W., and Cullen, J.L., 1999. A 0.5 million year record of millennial-scale climate variability in the North Atlantic. *Science,* 283:971–975.

Meese, D.A., Gow, A.J., Alley, R.B., Zielinsky, G.A., Grootes, P.M., Ram, M., Taylor, K.C., Mayewski, P.A., and Bolzan, J.F., 1997. The Greenland Ice Sheet Project 2 depth-age scale: methods and results. *J. Geophys. Res.,* 102:26411–26423.

Mikolajewicz, U., Crowley, T.J., Schiller, A., and Voss, R., 1997. Modeling teleconnections between the North Atlantic and North Pacific during the Younger Dryas. *Nature,* 387:384–387.

Oppo, D.W., and Fairbanks, R.G., 1989. Carbon isotope composition of tropical surface water during the past 22,000 years. *Paleoceanography,* 4:333–351.

Prell, W.L., Imbrie, J., Martinson, D.G., Morley, J.J., Pisias, N.G., Shackleton, N.J., and Streeter, H.F., 1986. Graphic correlation of oxygen isotope stratigraphy: application to the late Quaternary. *Paleoceanography,* 1:137–162.

Sarnthein, M., Pflaumann, U., Wang, P.X., and Wong, H.K. (Eds.), 1994. Preliminary Report on Sonne-95 Cruise "Monitor Monsoon" to the South China Sea. *Rep. Geol.–Palaeontol. Inst. Univ. Kiel.,* Vol. 68.

Sarnthein, M., Stattegger, K., Dreger, D., Erlenkeuser, H., Grootes, P., Haupt, B.J., Jung, S., Kiefer, T., Kuhnt, W., Pflaumann, U., Schäfer-Neth, C., Schulz, H., Schulz, M., Seidov, D., Simstich, J., van Kreveld, S., Vogelsang, E., Völker, A., and Weinelt, M., 2000. Fundamental modes and abrupt changes in North Atlantic circulation and climate over the last 60 ky—concepts, reconstruction and numerical modeling. *In* Schäfer, P, Ritzrau, W., Schlüter, M., and Thiede, J. (Eds.), *The Northern Atlantic: A Changing Environment:* Berlin (Springer), 365–410.

Sarnthein, M., and Tiedemann, R., 1989. Toward a high-resolution stable isotope stratigraphy of the last 3.4 million years: Sites 658 and 659 off northwest Africa. *In* Ruddiman, W., Sarnthein, M., et al., *Proc. ODP, Sci. Results,* 108: College Station, TX (Ocean Drilling Program), 167–185.

Sarnthein, M., and Tiedemann, R., 1990. Younger Dryas-style cooling events at glacial terminations I–VI at ODP Site 658: associated benthic δ^{13}C anomalies constrain meltwater hypothesis. *Paleoceanography,* 5:1041–1055.

Schulz, H., von Rad, U., and Erlenkeuser, H., 1998. Correlation between Arabian Sea and Greenland climate oscillations of the past 110,000 years. *Nature,* 393:54–57.

Shackleton, N.J., Berger, A., and Peltier, W.A., 1990. An alternative astronomical calibration of the lower Pleistocene timescale based on ODP Site 677. *Trans. R. Soc. Edinburgh: Earth Sci.,* 81:251–261.

Shackleton, N.J., and Opdyke, N.D., 1973. Oxygen isotope and paleomagnetic stratigraphy of equatorial Pacific core V28-238: oxygen isotope temperatures and ice volumes on a 10^5 year and 10^6 year scale. *Quat. Res.,* 3:39–55.

Shackleton, N.J., Sanchez-Goni, M.F., Pailler, D., and Y. Lancelot, 2002. Marine isotope Substage 5e and the Eemian interglacial. *Global Planet. Change,* 757:1–5.

Shipboard Scientific Party, 2000. Site 1144. *In* Wang, P., Prell, W.L., Blum, P., et al., *Proc. ODP, Init. Repts.,* 184, 1–97 [CD-ROM]. Available from: Ocean Drilling Program, Texas A&M University, College Station TX 77845-9547, USA.

Southon, J., Kashgarian, M., Fontugne, M., Metivier, B., and Yim, W.W.-S., 2002. Marine reservoir corrections for the Indian Ocean and southeast Asia. *Radiocarbon,* 44:167-180.

Stuiver, M., Reimer, P.J., Bard, E., Beck, J.W., Burr, G.S., Hughen, K.A., Kromer, B., McCormac, G., Van Der Plicht, J., and Spurk, M., 1998. INTCAL98 radiocarbon age calibration, 24,000-0 cal BP. *Radiocarbon,* 40:1041–1083.

Thierstein, H.R., Geitzenauer, K., Molfino, B., and Shackleton, N.J., 1977. Global synchroneity of late Quaternary coccolith datum levels: validation by oxygen isotopes. *Geology,* 5:400–404.

Thompson, P.R., Bé, A.W.H., Duplessy, J.-C., and Shackleton, N.J., 1979. Disappearance of pink-pigmented *Globigerinoides ruber* at 120,000 yr BP in the Indian and Pacific oceans. *Nature,* 280:554–558.

Tiedemann, R., 1994. Acht Millionen Jahre Klimageschichte von Nordwest Afrika und Paläoozeanographie des Angrenzenden Atlantiks: Hochauflösende Zeitreihen von ODP-Sites 658–661 [Ph.D. thesis]. Univ. Kiel, Germany.

Tiedemann, R., Sarnthein, M., and Shackleton, N.J., 1994. Astronomic timescale for the Pliocene Atlantic $\delta^{18}O$ and dust flux records of Ocean Drilling Program Site 659. *Paleoceanography,* 9:619–638.

van Kreveld, S., Sarnthein, M., Erlenkeuser, H., Grootes, P., Jung, S., Nadeau, M.J., Pflaumann, U., and Voelker, A., 2000. Potential links between surging ice sheets, circulation changes and the Dansgaard-Oeschger cycles in the Irminger Sea, 60–18 kyr. *Paleoceanography,* 15:425–442.

Vergnaud Grazzini, C., Saliège, J.F., Urrutiaguer, M.J., and Iannace, A., 1990. Oxygen and carbon isotope stratigraphy of ODP Hole 653A and Site 654: the Pliocene–Pleistocene glacial history recorded in the Tyrrhenian Basin (West Mediterranean). *In* Kastens, K.A., Mascle, J., et al., *Proc. ODP, Sci. Results,* 107: College Station, TX (Ocean Drilling Program), 361–386.

Voelker, A.H.L., Grootes, P.M., Nadeau, M.J., and Sarnthein, M., 2000. ^{14}C levels in the Iceland Sea from 25–53 kyr and their link to the Earth's magnetic field intensity. *Radiocarbon,* 42:437–452.

Wang, J., Zhao, Q., Cheng, X., Wang, R., and Wang, P., 2000. Age estimation of the mid-Pleistocene microtektite event in the South China Sea: a case showing the complexity of the sea-land correlation. *Chin. Sci. Bull.,* 45:2277–2280.

Wang, L., 2000. Isotopic signals in two morphotypes of *Globigerinoides ruber* (white) from the South China Sea: implications for monsoon climate change during the last glacial cycle. *Palaeogeogr., Palaeoclimatol., Palaeoecol.,* 161:381–394.

Wang, L., Sarnthein, M., Erlenkeuser, H., Grimalt, J., Grootes, P., Heilig, S., Ivanova, E., Kienast, M., Pelejero, C., and Pflaumann, U., 1999a. East Asian monsoon climate during the late Pleistocene: high-resolution sediment records from the South China Sea. *Mar. Geol.,* 156:245–284.

Wang, L., Sarnthein, M., Erlenkeuser, H., Grootes, P.M., Grimalt, J.O., Pelejero, C., and Linck, G., 1999b. Holocene variations in asian monsoon moisture: a bidecadal sediment record from the South China Sea. *Geophys. Res. Lett.,* 26:2889–2892.

Wang, L., Sarnthein, M., Grootes, P.M., and Erlenkeuser, H., 1999c. Millennial reoccurrence of century-scale abrupt events of east Asian monsoon: a possible heat conveyor for the global deglaciation. *Paleoceanography,* 14:725–731.

Wang, Y., Cheng, H., Edwards, R.L., An, Z.S., Wu, J.Y., Shen, C.-C., and Dorale, J.A., 2001. A high-resolution absolute-dated late Pleistocene monsoon record from Hulu Cave, China. *Science,* 294:2345–2348.

Wei, W., 1993. Calibration of upper Pliocene–lower Pleistocene nannofossil events with oxygen isotope stratigraphy. *Paleoceanography,* 8:85–99.

Yamei, H., Potts, R., Baoyin, Y., Zhentang, G., Deino, A., Wei, W., Clark, J., Guangmao, X., and Weiwen, H., 2000. Mid-Pleistocene Acheulean-like stone technology of the Bose Basin, South China. *Science,* 287:1622–1626.

Zhao, Q., Jian, Z., Li, B., Chen, X., and Wang, P., 1999. Middle Pleistocene microtektites in deep-sea sediments of the South China Sea. *Sci. China, Ser. D: Earth Sci.,* 42:531–535.

APPENDIX

Stable Isotope Data of *Globigerinoides ruber* (White)

Core, section, interval (cm)	Depth (mbsf)	Depth (mcd)	δ¹⁸O (‰ PDB) *Globigerinoides ruber*	±1δ¹⁸O	δ¹³C (‰ PDB) *Globigerinoides ruber*	±1δ¹³C	Age (ka)
184-1144C-							
1H-1, 6–8	0.06	0.06	–2.72	0.03	1.32	0.02	0.09
1H-1, 26–28	0.26	0.26	–2.46	0.01	1.34	0.01	0.44
1H-1, 48–50	0.48	0.48	–2.55	0.02	1.23	0.02	0.82
1H-1, 73–75	0.73	0.73	–2.56	0.02	1.25	0.01	1.26
1H-1, 96–98	0.96	0.96	–2.70	0.03	1.31	0.01	1.66
1H-1, 126–128	1.26	1.26	–2.52	0.02	1.39	0.01	2.18
1H-1, 143–145	1.43	1.43	–2.15	0.02	1.28	0.01	2.48
1H-2, 23–25	1.73	1.73	–2.76	0.02	1.41	0.01	3.00
1H-2, 48–50	1.98	1.98	–2.65	0.02	1.37	0.01	3.44
1H-2, 73–75	2.23	2.23	–2.19	0.04	1.17	0.02	3.88
1H-2, 93–95	2.43	2.43	–2.44	0.01	1.10	0.01	4.23
1H-2, 125–127	2.75	2.75	–2.53	0.02	1.26	0.01	4.78
1H-3, 23–25	3.23	3.23	–2.63	0.17	0.91	0.17	5.62
1H-3, 73–75	3.73	3.73	–2.24	0.01	1.22	0.01	6.49
1H-3, 96–98	3.96	3.96	–2.29	0.02	0.92	0.01	6.90
1H-3, 125–127	4.25	4.25	–2.35	0.02	0.95	0.01	7.40
1H-3, 143–145	4.43	4.43	–2.14	0.02	0.86	0.01	7.72
1H-4, 18–20	4.68	4.68	–2.38	0.02	0.87	0.01	8.15
1H-4, 48–50	4.98	4.98	–2.53	0.02	0.63	0.01	8.68
1H-4, 73–75	5.23	5.23	–2.03	0.01	0.69	0.00	9.11
1H-4, 103–105	5.53	5.53	–2.86	0.01	0.62	0.01	9.64
1H-4, 126–128	5.76	5.76	–2.50	0.03	0.54	0.01	10.04
1H-4, 143–145	5.93	5.93	–2.19	0.03	0.57	0.01	10.33
1H-5, 26–28	6.26	6.26	–2.29	0.01	0.69	0.01	10.91
184-1144B-							
2H-2, 143–145	3.03	6.41	–2.10	0.01	0.70	0.01	11.17
2H-3, 6–8	3.16	6.54	–2.22	0.01	0.73	0.01	11.40
184-1144C-							
1H-5, 73–75	6.73	6.73	–1.53	0.01	0.43	0.01	11.73
1H-5, 96–98	6.96	6.96	–1.99	0.02	0.92	0.01	11.92
184-1144B-							
2H-3, 73–75	3.83	7.21	–1.73	0.01	0.78	0.01	12.12
184-1144C-							
1H-5, 143–145	7.43	7.43	–1.66	0.01	0.59	0.01	12.29
184-1144B-							
2H-3, 128–130	4.38	7.76	–1.61	0.02	0.61	0.02	12.56
2H-3, 143–145	4.53	7.91	–1.51	0.01	0.56	0.01	12.68
2H-4, 23–25	4.83	8.21	–2.06	0.01	0.64	0.02	12.92
2H-4, 53–55	5.13	8.51	–2.11	0.01	0.79	0.01	13.17
2H-4, 73–75	5.33	8.71	–1.79	0.02	0.64	0.01	13.33
2H-4, 103–105	5.63	9.01	–1.72	0.01	0.52	0.02	13.57
2H-4, 126–128	5.86	9.24	–1.44	0.03	0.88	0.01	13.75
2H-4, 143–145	6.03	9.41	–1.55	0.01	0.41	0.02	13.89
2H-5, 23–25	6.33	9.71	–2.04	0.02	0.42	0.01	14.13
2H-5, 53–55	6.63	10.01	–2.04	0.03	0.43	0.01	14.38
2H-5, 73–75	6.83	10.21	–1.45	0.02	0.45	0.02	14.49
184-1144A-							
2H-2, 33–35	8.73	10.52	–1.14	0.03	0.41	0.01	14.66
2H-2, 53–55	8.93	10.72	–1.26	0.02	0.43	0.01	14.77
2H-2, 73–75	9.13	10.92	–1.23	0.02	0.51	0.01	14.88
2H-2, 103–105	9.43	11.22	–1.02	0.01	0.28	0.01	15.05
2H-2, 128–130	9.68	11.47	–1.24	0.03	0.50	0.01	15.19

Notes: PDB = Peedee belemnite standard. Only a portion of this table appears here. The complete table is available in ASCII.

Figure F1. Locations of ODP Leg 184 Sites 1144 through 1148 and position of SONNE-95 core 17940 in the northern South China Sea. 200-m isobath marks shelf edge.
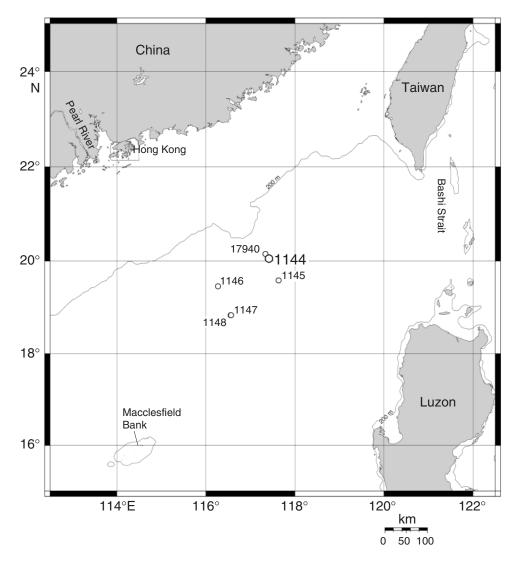
Figure F2. A. Oxygen isotope curve ($\delta^{18}O$ ratio vs. Peedee belemnite standard) of surface-dwelling planktonic foraminifer *Globigerinoides ruber* from Site 1144. Sampling density is listed in Table T1, p. 26. Dashed line at −2.6‰ indicates the Holocene average $\delta^{18}O$ level. Numbers are marine isotope stages and/or substages. YD = Younger Dryas. Asterisks = position of ^{14}C datings, line of open dots = microtektite layer. Solid vertical lines show position of hiatuses. Thin vertical lines below 235 mcd indicate core breaks. (Continued on next page.)
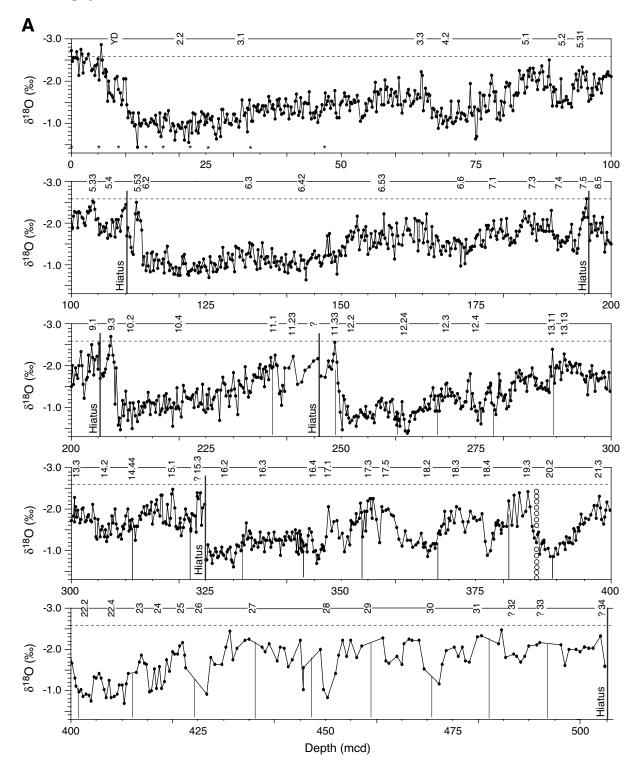
Figure F2 (continued). B. Carbon isotope record (δ¹³C ratio) of surface-dwelling planktonic foraminifer *G. ruber* from Site 1144. Roman numerals show position of glacial terminations.
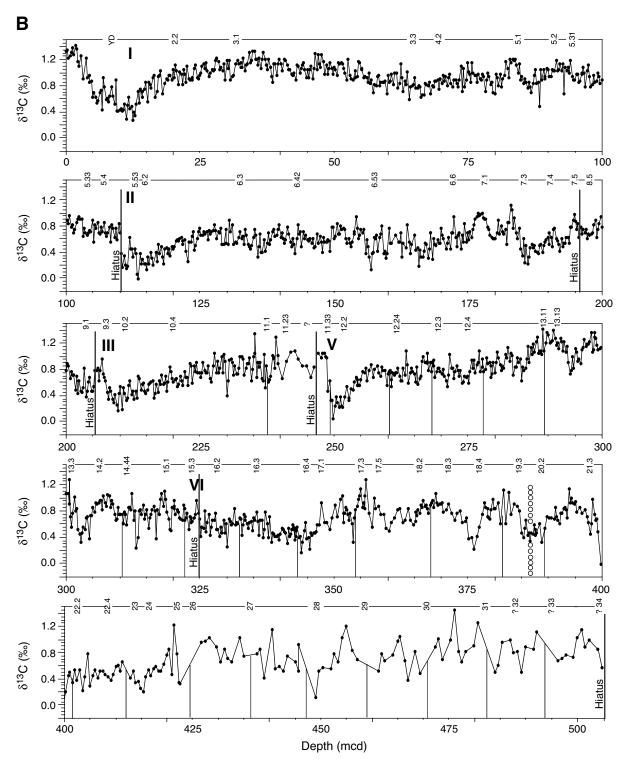
Figure F3. A. Oxygen isotope record of Greenland ice core GISP2 (Grootes and Stuiver, 1997) plotted against age. Numbers (1–23) indicate interstadials (IS). **B.** Site 1144 planktonic $\delta^{18}O$ record for the uppermost 108 mcd plotted against age. Thin lines define boundaries between marine isotope Stages (MIS) 1–5. Numbers (1–23) correlate planktonic $\delta^{18}O$ minima to IS in the GISP2 $\delta^{18}O$ record (A). "20K"IS marks $\delta^{18}O$ minimum that parallels a GISP2 warming near 20 ka. H1 through H6 identify high-salinity events coeval with North Atlantic Heinrich events. YD = Younger Dryas. Asterisks = position of ^{14}C-datings after conversion into calendar ages (see Table T1, p. 26). Massive arrow points toward a reduction in sea-surface salinity (SSS), interpreted as result of monsoon floods (1‰ = ~2‰ SSS).
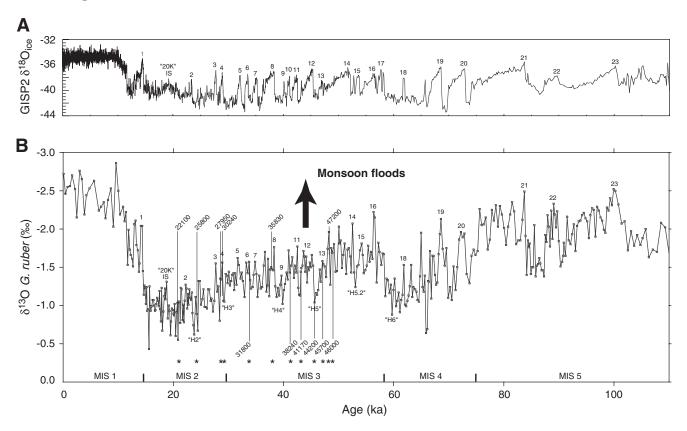
Figure F4. Site 1144 (**A**) oxygen and (**B**) carbon isotope curves (black lines) of planktonic foraminifer *G. ruber* (white) vs. age. Numbers indicate marine isotope stages based on a correlation with orbitally tuned age models of Marion Dufresne core MD90-0963 and ODP Sites 659/677 (Bassinot et al., 1994; Tiedemann et al., 1994) (gray curve behind δ18O record). Roman numerals = number of major glacial terminations. Double horizontal bars show extent of hiatuses (H). Biostratigraphic first (FO) and last (LO) occurrence datums are marked; open triangle = planktonic foraminifer first/last occurrence datum, solid triangle = nannoplankton and radiolarian first/last occurrence datum. Square = position of microtektite layer.
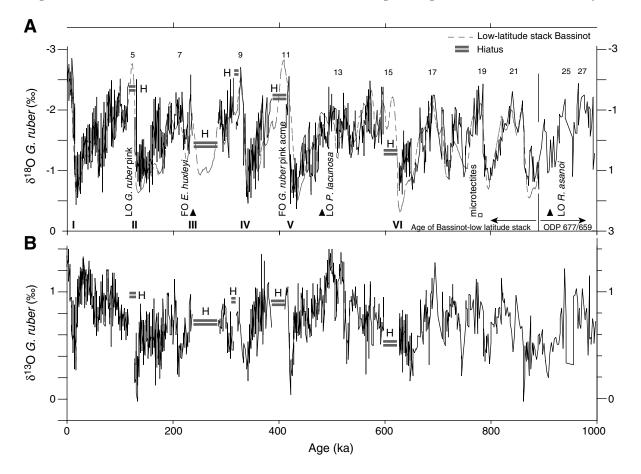
Figure F5. Sedimentation rates at Site 1144. Numbers indicate marine isotope Stages 1–33.

C. Bühring et al.
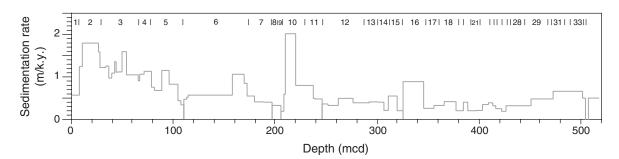Stable Isotope Stratigraphy, Site 1144

26

Table T1. Average sampling resolution for stable isotope analyses, Site 1144.

Depth (mcd)	N	Age range (ka)	Time span (k.y.)	Sampling resolution (yr)
0–110	438	0.09–116	117.31	268
110–196	341	128.0–235.41	107.41	315
196–239	175	286.0–372.96	86.96	497
239–247	12	372.96–414.04	41.08	3423
247–324	323	414.04–598.04	184.00	569
324–357	129	626.58–700.0	73.42	569
357–400	126	700.0–861.39	161.39	1280
400–422	44	861.39–941.52	80.13	1821
422–504	72	941.52–1100	158.48	2201
504–517	11	1960–1975.60	15.60	1418

Note: N = number of samples.

Table T2. AMS-^{14}C dates, Site 1144.

Core, section, interval (cm)	Depth (mcd)	Carbon (mg C)	Corrected pMC[†]	Conversion ^{14}C age (ka)	Error + (yr)	Error – (yr)	δ[–13]C (‰)	Calibrated age (ka)
184-1144A-								
1H-1, 25–30	0.735			1.721	60	–60		1.272*
1H-4, 25–30	5.24			9.487	65	–65		10.272*
2H-2, 25–30	10.47			13.571	75	–75		15.715*
2H-5, 25–30	14.97			18.115	80	–80		20.949*
2H-6, 103–105	17.22	1.1	13.09 ± 0.12	15.930	80	–80	1.45 ± 0.16‰	19.030*
4H-1, 126–128	22.23	0.9	9.33 ± 0.10	18.650	90	–90	0.19 ± 0.12‰	22.100*
4H-1, 25–30	27.53			22.430	110	–110		25.800[†]
4H-4, 41–43	32.21	0.6	4.31 ± 0.08	24.860	160	–150	–1.01 ± 0.08‰	27.950[†]
184-1144B-								
5H-1, 116–118	33.07	0.9	3.72 ± 0.07	26.050	160	–150	1.24 ± 0.21‰	30.240[†]
5H-5, 73–75	38.63	0.6	2.71 ± 0.07	28.570	210	–210	–2.38 ±0.13‰	31.800[†]
184-1144A-								
5H-5, 41–43	43.31	0.5	1.55 ± 0.07	33.070	390	–370	–1.15 ± 0.11‰	35.830[†]
184-1144B-								
6H-3, 143–145	47.23	0.7	1.11 ± 0.07	35.720	500	–470	–0.38 ± 0.18‰	38.420[†]
6H-5, 111–113	49.92	0.8	0.85 ± 0.06	37.890	570	–530	0.44 ± 0.11‰	41.170[†]
184-1144A-								
6H-4, 73–75	53.56	1.0	0.40 ± 0.05	43.950	1010	–900	0.68 ± 0.10‰	44.200[†]
6H-5, 73–75	55.06	0.8	0.34 ± 0.04	45.320	1130	–990	1.27 ± 0.12‰	45.700[‡]
6H-6, 73–75	56.56	0.7	0.28 ± 0.04	46.800	1370	–1170	–0.40 ± 0.07‰	47.200[‡]
6H-6, 143–145	57.26	1.0	0.35 ± 0.05	45.060	1190	–1140	2.07 ± 0.10‰	46.000[‡]

Notes: Samples in bold were dated in the Leibniz Laboratory of Kiel University, Germany; other dates are from Chen and Shyu (unpubl. data). All ^{14}C dates were corrected for assumed ^{14}C reservoir effect of –400 yr. * = age calibration with Calib 4.3 (Stuiver et al., 1998). [†] = approximate age calibration to GISP2 ages according to van Kreveld et al. (2000), [‡] = approximate age calibration to GISP2 ages according to Voelker et al. (2000), ^{14}C background = planktonic foraminifers from 110 mcd, MIS 5.4 (0.09/0.14% [14]C).

Table T3. Midpoint depths (mcd), δ¹⁸O values, ages, sedimentation rates, and names for marine isotope stages (MIS) and events, Site 1144.

Depth (mcd)	δ¹⁸O (‰)	Age (a)	Sedimentation rate (m/ky)	Event	Depth (mcd)	δ¹⁸O (‰)	Age (a)	Sedimentation rate (m/ky)	Event
0.06	−2.72	90	—		220.3	−0.76	347,500	2.02	MIS 10.4
6.73	−1.53	11,730	0.57	Top YD	236.95	−2.19	368,320	0.80	MIS 11.1
10.01	−2.04	14,375	1.24	IS 1	238.95	−1.04	372,440	0.49	MIS 11.23
26.19	−1.17	23,370	1.80	IS 2	245.63	−2.18	386,270	0.48	Hiatus top
26.89	−0.62	23,810	1.59	H2	246.33	−1.74	412,000	—	Hiatus bottom
31.62	−1.55	27,700	1.22	IS 3	248.89	−2.56	418,530	0.36	MIS 11.33
33.07	−1.56	28,890	1.22	IS 4	251.58	−0.63	426,000	0.36	MIS 12.22
33.57	−1.05	29,290	1.25	H3	262.18	−0.37	434,000	0.33	MIS 12.24
36.62	−1.62	31,720	1.26	IS 5	275.87	−0.6	461,470	0.49	MIS 12.4
38.63	−1.57	33,790	0.97	IS 6	291.23	−2.27	500,000	0.39	MIS 13.13
41.76	−1.7	36,660	1.09	IS 7	300.77	−2.06	523,000	0.41	MIS 13.3
44.02	−1.76	38,320	1.36	IS 8	306.52	−1.21	537,300	0.40	MIS 14.2
44.52	−1.1	38,770	1.11	H4	311.11	−1.51	559,500	0.21	MIS 14.44
45.52	−0.14	39,660	1.12	IS 9	318.86	−2.48	573,500	0.55	MIS 15.1
46.97	−1.72	40,960	1.12	IS 10	323.86	−2.38	598,000	0.20	MIS 15.3
48.73	−1.77	42,530	1.12	IS 11	324.62	−2.12	598,035	0.20	Hiatus top
52.9	−1.66	45,140	1.60	IS 12	324.86	−0.77	626,580	—	Hiatus bottom
53.56	−1.04	45,660	1.27	H5	326.12	−0.89	628,000	0.89	MIS 16.2
55.06	−1.58	47,090	1.05	IS 13	345.42	−0.69	649,500	0.89	MIS 16.4
64.77	−2.22	56,370	1.05	IS 16	355.79	−2.25	690,000	0.26	MIS 17.3
66.47	−1.67	58,230	0.91	IS 17	365.92	−0.85	720,500	0.33	MIS 18.2
70.33	−1.53	61,870	1.06	IS 18	377.17	−0.89	747,000	0.42	MIS 18.4
77.96	−2.13	68,610	1.13	IS 19	384.58	−2.43	783,700	0.20	MIS 19.3
81.21	−1.94	72,880	0.76	IS 20	388.83	−0.84	794,300	0.40	MIS 20.2
88.57	−2.49	83,750	0.68	IS 21	397.78	−2.31	838,500	0.20	MIS 21.3
95.42	−2.23	89,710	1.15	IS 22	399.28	−2.16	858,500	0.21	MIS 21.5
104.13	−2.5	100,250	0.83	IS 23	403.51	−0.89	870,500	0.35	MIS 22.2
106.81	−1.63	106,360	0.44	MIS 5.4	408.51	−0.85	883,240	0.39	MIS 22.4
110.05	−2.45	116,000	0.34	Hiatus top	413.89	−1.85	900,000	0.32	MIS 23
110.3	−1.68	128,000	—	Hiatus bottom	415.88	−0.99	908,000	0.25	MIS 24
112.05	−2.51	130,000	0.47	MIS 5.53	421.88	−2.18	940,000	0.19	MIS 25
114.55	−0.82	134,000	0.52	MIS 6.2 top	426.7	−0.9	955,000	0.32	MIS 26
133.42	−1.5	141,300	0.57	MIS 6.3	450.43	−0.81	1,004,000	0.48	MIS 28
143.53	−0.64	155,300	0.57	MIS 6.44	472.31	−1.16	1,037,000	0.66	MIS 30
157.95	−2.22	167,310	0.57	MIS 6.53	500.66		1,093,790	0.50	LO small Gephyrocapsa acme
168.55	−1.23	177,270	1.06	MIS 6.62	503.76	−2.32	1,100,000	0.50	MIS 34 top
172.16	−0.95	181,500	0.85	MIS 6.64					Hiatus
179.6	−2.07	194,970	0.55	MIS 7.1	506.82	−1.59	1,960,000	—	LO Discoaster brouweri/triradiatus
188.11	−2.07	215,930	0.41	MIS 7.3	517.56	−2.07	1,975,600	0.50	MIS 73
190.11	−1.34	220,870	0.40	MIS 7.4					
195.49	−2.58	234,170	0.40	MIS 7.5					
195.99	−1.58	235,410	0.40	Hiatus top					
196.24	−1.96	286,000	—	Hiatus bottom					
196.77	−2.17	287,630	0.33	MIS 8.5					
198.75	−1.31	293,720	0.33	MIS 8.6					
205.15	−2.52	313,350	0.33	MIS 9.1					
205.4	−1.68	318,700	—	MIS 9.2					
207.4	−2.71	329,030	0.19	MIS 9.3					
209.16	−0.46	342,000	0.59	MIS 10.2					

Notes: YD = Younger Dryas, IS = GISP2 interstadial equivalent. LO = last occurrence. Ages of last 110 k.y. are based on the Meese/Sowers timescale (Meese et al., 1994). H1–H6 = Heinrich event analog. Ages of MIS 6–34 are based on Shackleton et al. (1990) and Bassinot et al. (1994); nannofossil ages after to Shipboard Scientific Party (2000).

C. Bühring et al.
Stable Isotope Stratigraphy, Site 1144

29

Table T4. Biostratigraphic datums and age markers, Site 1144.

Event	Average depth (mcd) ± error	Age (ka)
LO *Globigerinoides ruber* **(pink)**	110.18 ± 0.13	124.8
FO *Emiliania huxleyi**	192.96 ± 0.13	228
FO *Globigerinoides ruber* **(pink)**	248.39 ± 0.25	417
LO *Pseudoemiliania lacunosa**	288.54 ± 0.12	478
Microtectite layer[†]	386.20 ± 0.03	791
LO Reticulofenestra *asanoi*[†]	417.23 ± 0.38	912
LO small *Gephyrocapsa* acme*	500.66 ± 0.38	1100
LO *Discoaster brouweri/triradiatus**	506.82 ± 2.04	1960

Note: Events in bold served as tie points for the age model; * = Shipboard Scientific Party (2000); † = Zhao (unpubl. data). Recalibrated ages are deduced from $\delta^{18}O$ stratigraphy at Site 1144.